PCP
PLANT & CELL PHYSIOLOGY

Identification of a Tri-Iron(III), Tri-Citrate Complex in the Xylem Sap of Iron-Deficient Tomato Resupplied with Iron: New Insights into Plant Iron Long-Distance Transport

Rubén Rellán-Álvarez[1], Justo Giner-Martínez-Sierra[2], Jesús Orduna[3], Irene Orera[1], José Ángel Rodríguez-Castrillón[2], José Ignacio García-Alonso[2], Javier Abadía[1,*] and Ana Álvarez-Fernández[1]

[1]Department of Plant Nutrition, Aula Dei Experimental Station, CSIC, PO Box 13034, E-50080 Zaragoza, Spain
[2]Department of Physical and Analytical Chemistry, University of Oviedo, c/Julian Clavería 8, E-33006 Oviedo, Spain
[3]New Organic Materials Unit, Institute of Materials Science of Aragón, CSIC-University of Zaragoza, c/Pedro Cerbuna 12, E-50009 Zaragoza, Spain
*Corresponding author: E-mail, jabadia@eead.csic.es; Fax, +34-976716145
(Received September 24, 2009; Accepted November 18, 2009)

Regular Paper

The identification of Fe transport forms in plant xylem sap is crucial to the understanding of long-distance Fe transport processes in plants. Previous studies have proposed that Fe may be transported as an Fe–citrate complex in plant xylem sap, but such a complex has never been detected. In this study we report the first direct and unequivocal identification of a natural Fe complex in plant xylem sap. A tri-Fe(III), tri-citrate complex (Fe_3Cit_3) was found in the xylem sap of Fe-deficient tomato (*Solanum lycopersicum* Mill. cv. 'Tres Cantos') resupplied with Fe, by using an integrated mass spectrometry approach based on exact molecular mass, isotopic signature and Fe determination and retention time. This complex has been modeled as having an oxo-bridged tri-Fe core. A second complex, a di-Fe(III), di-citrate complex was also detected in Fe–citrate standards along with Fe_3Cit_3, with the allocation of Fe between the two complexes depending on the Fe to citrate ratio. These results provide evidence for Fe–citrate complex xylem transport in plants. The consequences for the role of Fe to citrate ratio in long-distance transport of Fe in xylem are also discussed.

Keywords: Iron deficiency • Iron-citrate • Mass spectrometry • Xylem sap • Iron transport.

Abreviations: B3LYP, hybrid density functional method; DFT, density functional theory; ESI-MS, electrospray ionization-mass spectrometry; EXAFS, extended X-ray absorption fine structure; HILIC, hydrophilic interaction liquid chromatography; HPLC, high performance liquid chromatography; IDA, isotope dilution analysis; IPD, isotope pattern deconvolution; LOD, linits of detection; NA, nicotianamine; Q-ICP-MS, quadrupole-inductively coupled plasma-mass spectrometry; TOF, time of flight; XANES, X-ray absorption near edge structure; SXRF, synchroton X-ray fluorescence.

This paper is dedicated to the memory of Dr. Arthur Wallace, a pioneer in the study of plant iron nutrition.

Introduction

The mechanisms of long-distance Fe transport in plants have remained elusive until now. In the case of xylem sap, Fe is assumed to be transported as complexed forms, because free ionic forms [Fe(II) and Fe(III)] can be toxic and are also prone to undergo precipitation at the neutral or slightly acidic pH values typical of xylem sap. Increases in carboxylate concentrations in plant xylem exudates with Fe deficiency were reported in several papers published in the 1960s by Brown and co-workers. Iron was first suggested to be transported bound to malate (Tiffin and Brown 1962), but later citrate (Cit), which also increases markedly in stem exudates of many plant species when Fe-deficient (Brown 1966) and co-migrates with Fe during paper electrophoresis (Tiffin 1966a, Tiffin 1966b, Tiffin 1970, Clark et al. 1973), was considered the most likely candidate for Fe transport.

The identity of Fe–Cit complexes in the xylem sap has only been hypothesized by means of in silico calculations using total concentrations of possible Fe complexing agents (including carboxylates) and Fe, and the known stability constants of Fe-containing complexes, always assuming that chemical equilibrium was achieved. Using this approach, several Fe–Cit species were predicted to be the most abundant Fe complexes in the xylem sap whereas other potential plant metal chelators such as nicotianamine (NA) were ruled out (von Wirén et al. 1999, Rellán-Álvarez et al. 2008) as possible xylem Fe carriers. NA function as an Fe chelator might be restricted to the cytoplasm and in Fe phloem loading (Curie et al. 2008). Citrate recently has been found by using molecular biology techniques to play a role in long-distance Fe transport. Xylem sap loading

Plant Cell Physiol. 51(1): 91–102 (2010) doi:10.1093/pcp/pcp170, available online at www.pcp.oxfordjournals.org

of Cit is seriously disrupted in two mutants, AtFRD3 (Durrett et al. 2007) and OsFRDL1 (Yokosho et al. 2009). These mutants display increased Fe-deficiency symptoms that have been associated with decreased efficiency of Fe translocation into the root vasculature.

Fe–Cit chemistry in aqueous solutions is very complex and a large number of chemical species may occur, depending on many factors (Spiro et al. 1967a, Spiro et al. 1967b, Pierre and Gautier-Luneau 2000, Gautier-Luneau et al. 2005). Direct proof of the presence of Fe–Cit complexes in xylem sap has not been obtained so far. Difficulties in detecting Fe–Cit species in xylem sap may arise for different reasons. First, both pH and Fe:Cit ratio values are known to affect markedly Fe–Cit speciation in standard aqueous solutions (Gautier-Luneau et al. 2005). Therefore, when analysis is carried out at pH values too acidic or basic (e.g. during HPLC), the speciation of Fe–Cit complexes could change and species occurring in the original xylem sample may no longer be present after chromatography. Second, analytical techniques such as mass spectrometry (MS), which have been used successfully to identify other metal complexes in the xylem sap (Ouerdane et al. 2006, Xuan et al. 2006), usually involve ionization steps (with high temperatures and voltages) that may be too harsh for relatively labile compounds such as Fe–Cit complexes. Furthermore, in most plant species the total Fe concentration in the xylem sap is in the μM range, and consequently the concentrations of the possible Fe–Cit complexes are expected to be very low.

Molecular biology approaches have provided a breadth of information about metal, metal chelator and metal complex transporters (Briat et al. 2007, Kim and Guerinot 2007, Palmer and Guerinot 2009). However, the elucidation of the molecular identity of metal complexes in plant compartments is still one of the biggest challenges in plant metal transport (Hider et al. 2004). The molecular identification of metal complexes has been tackled by two different types of technique. First, the use of highly selective and sensitive molecular and metal-specific techniques such as integrated MS (Meija et al. 2006) has been used (Ouerdane et al. 2006, Xuan et al. 2006), especially in plant fluids (e.g. xylem or phloem) where direct analysis can be carried out. Second, X-ray absorption spectroscopy, extended X-ray absorption fine structure (EXAFS) and X-ray absorption near edge structure (XANES) (Sarret et al. 2002, Küpper et al. 2004) and synchrotron X-ray fluorescence (SXRF) (Punshon et al. 2009) techniques have been applied to study metal speciation in some plant materials. The combination of metal complex elucidation techniques and molecular biology approaches should give a better picture of plant metal transport.

In this study we have used HPLC coupled to electrospray time of flight mass spectrometry (HPLC–ESI-TOFMS) and inductively coupled plasma mass spectrometry (HPLC–ICP-MS) to detect naturally occurring Fe complexes in xylem sap. Analysis conditions were kept as conservative as possible in order to maintain unaltered natural Fe species occurring in the xylem sap. With this approach we have succesfully identified a tri-Fe(III), tri-citrate complex (Fe_3Cit_3) in the xylem sap of Fe-deficient tomato plants after short-term Fe resupply. This complex has been modeled as an oxo-bridged tri-Fe(III) tri-Cit complex. A second Fe–Cit complex, the binuclear Fe(III)–Cit species Fe_2Cit_2, was only detected in Fe–Cit standard solutions along with the Fe_3Cit_3 complex, with the balance between the two complexes depending on the Fe:Cit ratio.

Results

Analysis of Fe–Cit standard solutions by integrated MS

A method to separate and identify Fe–Cit complexes was developed by analyzing Fe–Cit solutions with Fe and Cit concentrations, Fe:Cit ratios and pH values (5.5) typical of xylem sap, using HPLC and integrated MS (ESI-TOFMS and ICP-MS). In all experiments, ESI-TOFMS spectra were searched for any molecular ion having the characteristic Fe isotopic signatures, including molecular ions previously detected by ESI-MS in high concentration Fe–Cit solutions (100 mM Fe:1 M Cit) (Gautier-Luneau et al. 2005). The four different Fe stable isotopes were determined in the HPLC–ICP-MS runs. The method to determine Fe–Cit complexes was designed by optimizing first the electrospray ionization conditions, and then developing appropriate HPLC separation conditions. Throughout this study we used ^{54}Fe, ^{57}Fe and ^{nat}Fe, the latter being Fe with the natural isotopic composition: 5.85, 91.75, 2.12 and 0.28% of ^{54}Fe, ^{56}Fe, ^{57}Fe and ^{58}Fe, respectively.

Electrospray ionization conditions for Fe–Cit complexes were optimized to avoid in-source fragmentation using direct injection of a 1:10 ^{nat}Fe–Cit solution (100 μM ^{nat}Fe). Optimal ESI values for capillary exit, skimmer 1 and hexapole RF voltages were −57.1, −39.1 and 145.2 V, respectively. These values correspond to softer ESI conditions than those usually applied to low molecular weight analytes (in the 100–600 m/z range). In all conditions tested, citrate gave a strong signal at the $[CitH]^-$ mass-to-charge ratio (m/z) of 191.0 (**Supplementary Fig. 1A, B**; see inset for isotopic signature). With these soft conditions, a 10-fold increase in ionization efficiency was achieved for a m/z 366.4 signal that showed the characteristic isotopic signature of a double charged, three Fe atom-containing molecular ion. This signal can be assigned to the $[Fe(III)_3Cit_3H]^{2-}$ molecular ion (**Supplementary Fig. 1A, B**; see inset for isotopic signature). Furthermore, a second molecular ion with the characteristic isotopic signature of a double charged, three Fe atom-containing molecular ion was detected at m/z 375.4 (**Supplementary Fig. 1B**; see inset for isotopic signature). This signal can be assigned to the $[Fe(III)_3OCit_3H_3]^{2-}$ ion. The 9 m/z difference from $[Fe(III)_3Cit_3H]^{2-}$ was assigned to correspond to a labile ligand such as aquo OH_2, hydroxo OH^- or oxo O^{2-} (Gautier-Luneau et al. 2005). Both Fe–Cit molecular ions were previously reported to occur at neutral pH values and at similar Fe:Cit ratios (Gautier-Luneau et al. 2005). The relative intensities of the different peaks did not match those found by Gautier-Luneau et al. (2005), probably due to differences

in MS devices and solution pH values (at least one pH unit of difference). Conversely, signals at m/z 300.4 and 271.9 appeared under standard ESI conditions (**Supplementary Fig. 1A**) but they were significantly reduced after ESI optimization (**Supplementary Fig. 1B**), suggesting that they may correspond to in-source fragmentation products (mainly due to decarboxylation processes, very common in this kind of compound) of the Fe_3Cit_3 produced at higher voltage values.

HPLC separation conditions were also optimized to obtain a good separation of the Fe–Cit complexes from other matrix components (e.g. Cit) that could interfere in the ESI process. The range of HPLC options available was limited, since: (i) both Cit and Fe–Cit complexes are compounds with a high polarity; (ii) it is mandatory to maintain xylem sap-typical pH values during chromatography; (iii) the method must be suitable for ESI-TOFMS and ICP-MS detection. Different approaches, including several column types, elution programs and eluents—acetonitrile and methanol—were tested. The best results were obtained with a zwitterionic hydrophilic interaction column (ZIC-HILIC; Sequant), previously used to separate polar Fe compounds such as Fe(II)–NA, Fe(III)–deoxymugineic acid [Fe(III)–DMA] and others (Xuan et al. 2006). Two parallel systems, an HPLC–ICP-MS and an HPLC–ESI-TOFMS, were used to gain knowledge about atomic and molecular identity, respectively. Experiments were carried out with ^{54}Fe–Cit and also with ^{nat}Fe–Cit.

HPLC–ICP-MS experiments were carried out using ^{54}Fe–Cit solutions (100 µM ^{54}Fe:1 mM Cit) to avoid ^{nat}Fe background from the HPLC system, which could be significant when determining very low concentrations of Fe by ICP-MS. Iron-54 molar flow chromatograms showed only two well-defined Fe peaks at 32.1 and 38.3 min (**Fig. 1A**) that were also observed using UV detection (**Supplementary Fig. 2A**). Using ESI-TOFMS detection, only four molecular ions with characteristic ^{54}Fe isotopic signatures (see below for identification) were found in the chromatogram, two of them at 27.1 min (241.9 and 484.9 m/z) and two more at 32.9 min (363.4 and 372.4 m/z) (**Fig. 1B**), and a UV signal was also found for these peaks (**Supplementary Fig. 2B**). The 5-min differences in retention time between HPLC–ESI-TOFMS and HPLC–ICP-MS analyses are due to the different HPLC devices used (Waters and Agilent, respectively), as judged by the shift in UV detection traces (**Supplementary Fig. 2**). A 5 mM Cit solution was also injected

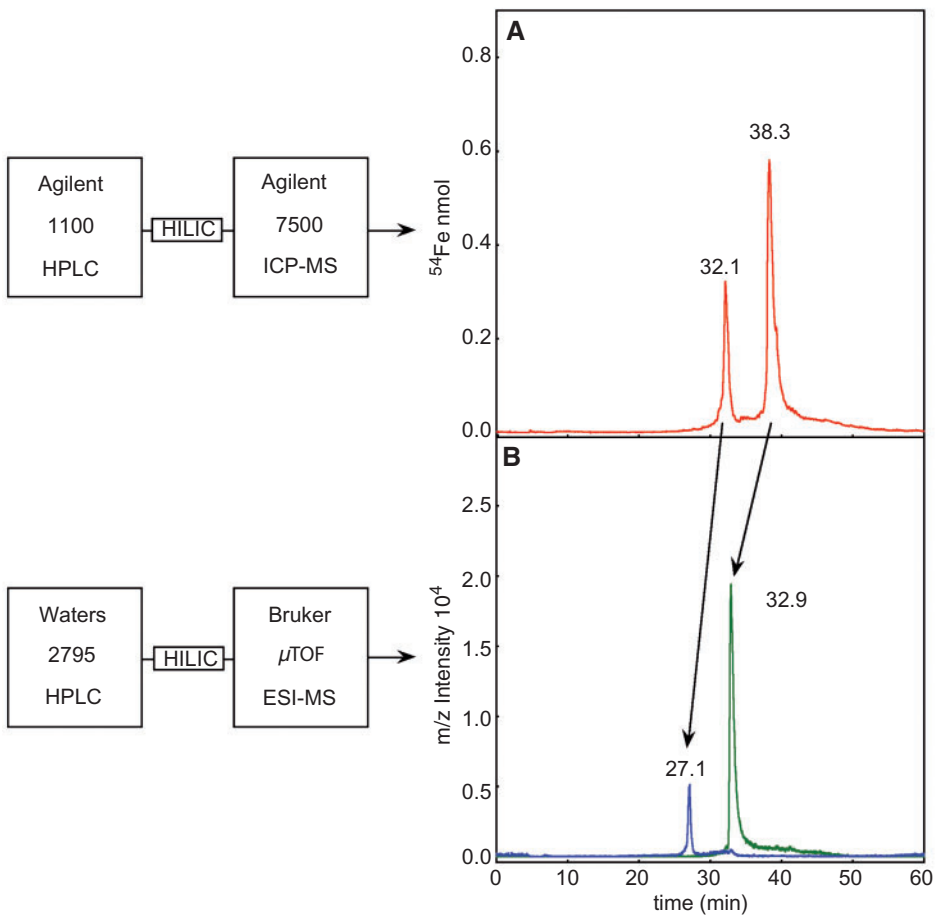

Fig. 1 HPLC–ICP-MS (A) and HPLC–ESI-TOFMS (B) chromatograms of a ^{54}Fe–Cit standard solution (Fe:Cit ratio 1:10, 100 µM ^{54}Fe, pH 5.5, in 50% mobile phase B) showing peaks corresponding to Fe complexes. HPLC–ESI-TOFMS traces (B) are the sum of molecular ions at m/z values 241.93 and 484.87 (±0.05; blue line) and 363.40 and 372.40 (±0.05; green line).

and no Fe–Cit complexes were found in the HPLC–ESI-TOFMS chromatogram, indicating that complexes found were not formed de novo during the chromatographic run.

With this HPLC method a complete separation of Fe–Cit complexes from Cit was reached, since Cit eluted as a broad peak at 5–9 min (m/z trace at 191.1, not included in **Fig. 1B**; **Supplementary Fig. 3A**). Other Fe complexes putatively occurring in plant tissues, such as Fe(III)–NA and Fe(III)–DMA, elute at retention times lower than 20 min (**Supplementary Fig. 3B, C**).

Identification of an Fe_2Cit_2 complex in Fe–citrate standard solutions

When using ^{54}Fe–Cit, the Fe peak at 27.1 min in HPLC–ESI-TOFMS, showed signals at m/z 241.9 and 484.9 (**Fig. 1B**) with Fe isotopic signatures characteristic of two ^{54}Fe atom-containing molecular ions, the first double charged (**Fig. 2A, Table 1**) and the second single charged (**Supplementary Fig. 4A**). Based on these exact mass and isotopic pattern data, the SigmaFit™ algorithm (Ojanperä et al. 2006) proposed $^{54}Fe_2C_{12}H_8O_{14}$ and $^{54}Fe_2C_{12}H_9O_{14}$ as the most accurate formulae, corresponding to the two Fe, two Cit molecular ions $[^{54}Fe(III)_2Cit_2]^{2-}$ and $[^{54}Fe(III)_2Cit_2H]^{-}$, respectively (**Table 1**); these molecular ions were previously found in concentrated Fe–Cit standards (Gautier-Luneau et al. 2005). The fit of the experimental and theoretical isotopic signatures of the $[^{54}Fe(III)_2Cit_2]^{2-}$ molecular ion at m/z 241.9 is shown in **Fig. 2A** and **B**, respectively. A good fit was also found for the ion $[^{54}Fe(III)_2Cit_2H]^{-}$ at m/z 484.9 (**Supplementary Fig. 4A, B**).

Further confirmation of the molecular identity of the Fe_2Cit_2 complex was obtained by analyzing ^{nat}Fe–Cit standard solutions by HPLC–ESI-TOFMS, taking advantage of the characteristic ^{nat}Fe isotopic signature. The Fe peak at 27.1 min in HPLC–ESI-TOFMS showed signals at m/z 243.9 and 488.9, characteristic of two ^{nat}Fe atom-containing molecular ions, the first double charged and the second single charged (**Fig. 2C, Supplementary Fig. 4C, Table 1**). The differences in m/z values found using ^{54}Fe and ^{nat}Fe (92% ^{56}Fe) were those expected for two Fe atom-containing molecular ions (2 and 4 m/z difference for a double and a single charged ion, respectively). The SigmaFit™ algorithm (Ojanperä et al. 2006) proposed $^{nat}Fe_2C_{12}H_{18}O_{14}$ and $^{nat}Fe_2C_{12}H_9O_{14}$ as the most accurate formulae corresponding to the molecular ions $[^{nat}Fe_2Cit_2]^{2-}$ and $[^{nat}Fe_2Cit_2H]^{-}$ (**Table 1**). The fit of the experimental and theoretical isotopic signatures of the $[^{nat}Fe_2Cit_2]^{2-}$ molecular ion (for the ^{56}Fe signal at m/z 243.9) is shown in **Fig. 2C** and **D**, respectively. A good fit was also found for the molecular ion $[^{nat}Fe_2Cit_2H]^{-}$ (for the ^{56}Fe signal at 488.9 m/z; **Supplementary Fig. 4C, D**).

Identification of an Fe_3Cit_3 complex in Fe–citrate standard solutions

The Fe peak at 32.9 min in HPLC–ESI-TOFMS analysis of ^{54}Fe–Cit solutions (**Fig. 1B**) showed signals at m/z 372.4 and 363.4, with isotopic signatures characteristic of three ^{54}Fe atom-containing

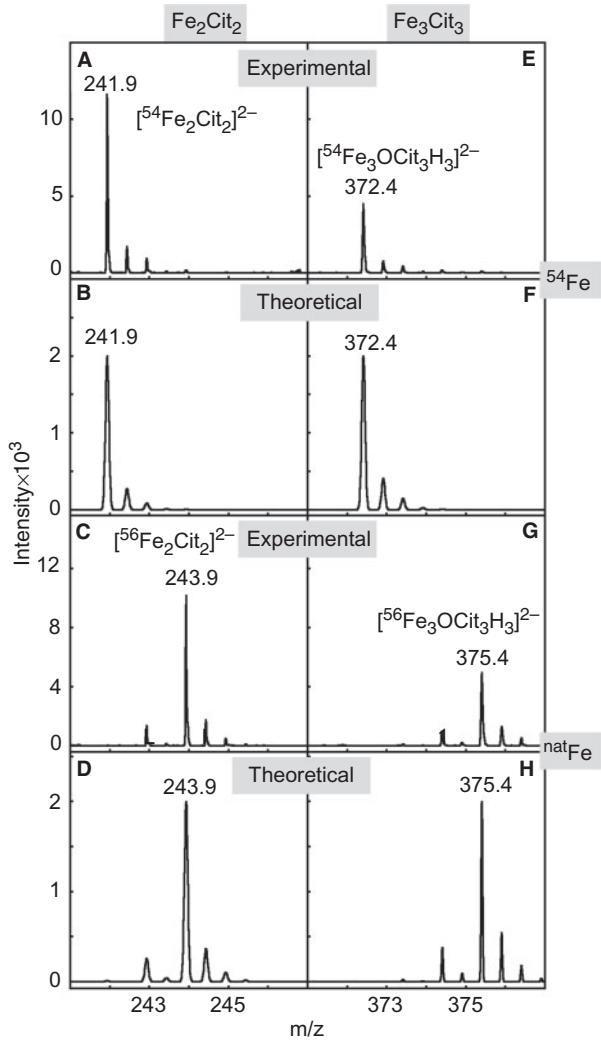

Fig. 2 Experimental (A, C, E, G) and theoretical (B, D, F, H) isotopic signatures of the molecular ions associated with Fe_2Cit_2 and Fe_3Cit_3, $[Fe_2Cit_2]^{2-}$ and $[Fe_3OCit_3H_3]^{2-}$, respectively. Experimental data are zoomed ESI-TOF mass spectra of the Fe_2Cit_2 and Fe_3Cit_3 chromatographic peaks found when using ^{54}Fe (A, E) and ^{nat}Fe (C, G).

molecular ions, both of them double charged (**Fig. 2E, Supplementary Fig. 4E, Table 1**). The algorithm proposed $^{54}Fe_3C_{18}H_{15}O_{22}$ and $^{54}Fe_3C_{18}H_{13}O_{21}$ as the most accurate formulae, corresponding to the three Fe-, three Cit- molecular ions $[^{54}Fe_3OCit_3H_3]^{2-}$ and $[^{54}Fe_3Cit_3H]^{2-}$ (**Table 1**). The fit of the experimental and theoretical isotopic signatures of the $[^{54}Fe_3OCit_3H_3]^{2-}$ molecular ion at m/z 372.4 is shown in **Fig. 2E** and **F**, respectively. The same occurs with the ion $[^{54}Fe_3Cit_3H]^{2-}$ at m/z 363.4 (**Supplementary Fig. 4E, F**).

Further confirmation of the molecular identity of the Fe_3Cit_3 complex was obtained by analyzing ^{nat}Fe–Cit standard solutions. The peak at 32.9 min shows signals at m/z 375.4 and 366.4, characteristic of three ^{nat}Fe atom-containing molecular ions (**Fig. 2G, Table 1**); these values were 3 m/z higher than those found using ^{54}Fe. The algorithm proposed $^{nat}Fe_3C_{18}H_{15}O_{22}$ and

Table 1 Experimental ESI-TOFMS molecular ion data and parameters used to identify the molecular formulae of the Fe–Cit complexes in standard solutions and tomato xylem sap

Measured m/z	$^{56}Fe/^{54}Fe$ (Fe atoms)[a]	Charge[b]	Molecular formula	Calculated m/z	Error m/z (ppm)	SigmaFit™ value	Molecular ion
			Standard solutions				
241.9362	–	−2	$^{54}Fe_2C_{12}H_8O_{14}$	241.9359	2.1	0.0234	$[^{54}Fe_2Cit_2]^{2-}$
484.8781	–	−1	$^{54}Fe_2C_{12}H_9O_{14}$	484.8790	1.8	0.0157	$[^{54}Fe_2Cit_2H]^{-}$
372.4119	–	−2	$^{54}Fe_3C_{18}H_{15}O_{22}$	372.4127	2.3	0.0273	$[^{54}Fe_3OCit_3H_3]^{2-}$
363.4068	–	−2	$^{54}Fe_3C_{18}H_{13}O_{21}$	363.4074	1.4	0.0106	$[^{54}Fe_3Cit_3H]^{2-}$
243.9311	7.4 (2)	−2	$^{nat}Fe_2C_{12}H_8O_{14}$	243.9311	1.7	0.0165	$[^{nat}Fe_2Cit_2]^{2-}$
488.8705	7.1 (2)	−1	$^{nat}Fe_2C_{12}H_9O_{14}$	488.8696	2.6	0.0214	$[^{nat}Fe_2Cit_2H]^{-}$
375.4047	5.2 (3)	−2	$^{nat}Fe_3C_{18}H_{15}O_{22}$	375.4057	1.7	0.0284	$[^{nat}Fe_3OCit_3H_3]^{2-}$
366.3994	5.2 (3)	−2	$^{nat}Fe_3C_{18}H_{13}O_{21}$	366.4004	2.0	0.0294	$[^{nat}Fe_3Cit_3H]^{2-}$
			Xylem sap				
372.4097	–	−2	$^{54}Fe_3C_{18}H_{15}O_{22}$	372.4057	8.2	0.0283	$[^{54}Fe_3OCit_3H_3]^{2-}$
375.4045	5.56 (3)	−2	$^{nat}Fe_3C_{18}H_{15}O_{22}$	375.4057	6.8	0.0197	$[^{nat}Fe_3OCit_3H_3]^{2-}$

The parameters used to assess the accuracy of molecular formulae were exact molecular mass and isotopic signatures, with exact mass errors of <10 ppm, and a SigmaFit™ value of <0.03 (Ojanperä et al. 2006) (see Materials and Methods). Data are means of at least three independent HPLC runs.

[a]The $^{56}Fe/^{54}Fe$ ratio was used to determine the number of Fe atoms in the molecule. Theoretical $^{56}Fe/^{54}Fe$ ratios for molecules containing two or three Fe atoms are 7.9 and 5.3, respectively.

[b]The ion charge was determined by the m/z isotope difference within a given molecule. Differences of 1.0 and 0.5 m/z indicate molecular ion charges of 1 and 2, respectively.

$^{nat}Fe_3C_{18}H_{13}O_{21}$ and as the most accurate formulae, corresponding to the three Fe-, three Cit- molecular ions $[^{nat}Fe_3OCit_3H_3]^{2-}$ and $[^{nat}Fe_3Cit_3H]^{2-}$ (**Table 1**). The fit of the experimental and theoretical isotopic signatures of the $[^{nat}Fe_3OCit_3H_3]^{2-}$ molecular ion (for the ^{56}Fe signal at m/z 375.4) is shown in **Fig. 2G** and **H**, respectively. A good fit was also found for the ion $[^{nat}Fe_3Cit_3H]^{2-}$ (for the ^{56}Fe signal at 366.4 m/z; **Supplementary Fig. 4G, H**).

Iron to citrate ratios drive the balance between Fe_2Cit_2 and Fe_3Cit_3 in standard solutions

To assess the influence of the Fe:Cit ratio on the balance of Fe–Cit complexes, standard solutions with Fe:Cit ratios of 1:1, 1:10, 1:100 and 1:500 (at 100 µM Fe) were analyzed by HPLC–ESI-TOFMS and HPLC–ICP-MS, always at the pH value typical of xylem sap. Both detection systems show that high Fe:Cit ratios favor the formation of Fe_3Cit_3, whereas lower Fe:Cit ratios lead to the formation of Fe_2Cit_2 (**Fig. 3**). With Fe:Cit ratios >1:10, Fe_3Cit_3 would account for >75% of the total complexed Fe, whereas with Fe:Cit ratios <1:75, Fe_2Cit_2 would account for >75% of the total. In the range between these ratios both complexes would be present. In all cases, no other Fe-containing peaks different from Fe_2Cit_2 and Fe_3Cit_3 were found by HPLC–ICP-MS or HPLC–ESI-TOFMS (**Supplementary Fig. 5**).

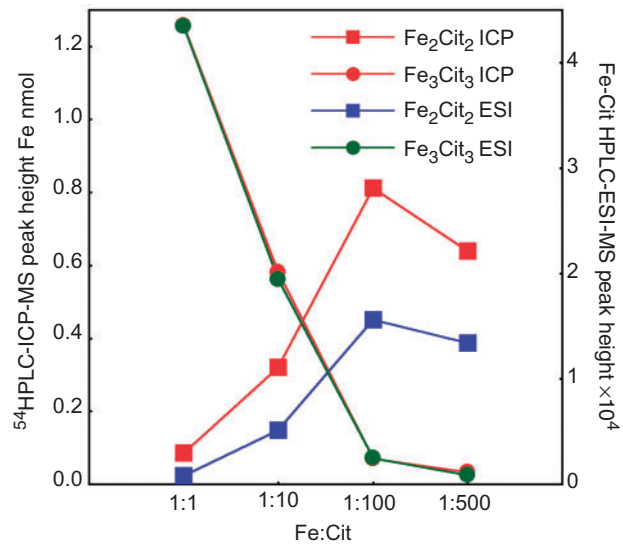

Fig. 3 Effect of the Fe:Cit ratio on the Fe_2Cit_2 and Fe_3Cit_3 balance. Data are chromatographic peak maximum heights obtained with ICP-MS and ESI-TOFMS detection. ^{54}Fe–Cit standard solutions with Fe:Cit ratios of 1:1, 1:10, 1:100 and 1:500 (at 100 µM ^{54}Fe, pH 5.5 in 50% mobile phase B) were used.

Quantification of Fe–Cit complexes in Fe–citrate standard solutions

We attempted to quantify the amount of Fe associated with the Fe–Cit complexes found in ^{54}Fe–Cit solutions by using HPLC–ICP-MS ^{54}Fe molar flow chromatograms. The sum of the Fe–Cit complexes Fe_2Cit_2 and Fe_3Cit_3 accounted for approximately 60% ($n = 4$) of the total injected Fe. However, only 67% of the Fe was eluted from the HPLC. Therefore, the Fe contained in the Fe_2Cit_2 and Fe_3Cit_3 peaks accounted for 91% of the eluted Fe. When the analysis was carried out with longer run times

Table 2 Xylem sap pH, Fe and citrate concentrations, Fe:Cit ratios and Fe_3Cit_3 and Fe_2Cit_2 complexes (in % of the chromatographically eluted Fe), in Fe-sufficient (+Fe), Fe-deficient (−Fe) and Fe-deficient tomato plants resupplied with Fe–*o,o*EDDHA for 12 h (Fe-resupplied)

Fe status	Fe in solution (μM)	pH	Fe (μM)	Cit (μM)	Fe:Cit	Fe_3Cit_3 (%)	Fe_2Cit_2 (%)
+Fe	45	5.8±0.1	19.9±2.6	11.6±6.6	1:0.6	bld[a]	bld
−Fe	$0+HCO_3^-$	5.8±0.1	5.4±4.4	165±9.2	1:31	bld	bld
Fe-resupplied	$(0+HCO_3^-)+45$	5.5±0.1	121.0±13.7	172.2±12.6	1:1.4	71[b]	bld

Data are means±SE of at least three independent samples.
[a]bld: below detection limit.
[b]Since only 25% of the total injected Fe was eluted from the column, this percentage corresponds to 16% of the total injected Fe.

a broad Fe peak eluted at approximately 70 min, indicating that at least an additional Fe form either occurred in the original sample or was formed from Fe–Cit complexes during the LC run. The UV–visible spectra of this peak suggest that it may correspond to Fe-oxyhydroxides.

The Fe_3Cit_3 complex is present in the xylem sap of Fe-deficient tomato plants resupplied with Fe

We analyzed xylem sap to look for the presence of possible Fe–Cit complexes by the optimized methodology described above. We used xylem of Fe-sufficient, Fe-deficient and Fe-deficient plants resupplied with Fe–ethylenediamine-*N*-*N*′ bis(*o*-hydroxyphenylacetic) acid (*o,o*EDDHA) for 6, 12 and 24 h, where Fe concentrations were 19.9±2.6, 5.4±4.4, 42.9±3.7, 121.0±13.7 and 43.5±9.1 μM ($n=4$), respectively (**Table 2**). The xylem sap of plants resupplied for 12 h was chosen for further studies, since they have the highest concentrations of Fe. These xylem sap samples showed a major ^{54}Fe peak in HPLC–ICP-MS at 39.5 min (**Fig. 4A**). When using HPLC–ESI-TOFMS, an Fe peak eluted at 34.1 min and showed signals at m/z 372.4 or 375.4 when the Fe source was ^{54}Fe-*o,o*EDDHA or ^{nat}Fe-*o,o*EDDHA, respectively (**Fig. 4B, C**). The retention time difference between HPLC–ICP-MS and HPLC–ESI-TOFMS was due to the use of different HPLC systems as explained above. Based on this exact mass and the isotopic pattern data (see insets of **Fig. 4B, C**), the algorithm proposed $Fe_3C_{18}H_{15}O_{22}$ as the more accurate molecular formula (**Table 1**; ^{56}Fe signal m/z error 6.8 ppm and SigmaFit™ value 0.0197), corresponding to the Fe_3Cit_3 molecular ion $[Fe_3O(Cit)_3H_3]^{2-}$ also found in the Fe–Cit standards (**Figs. 1, 2**). The approximately 1-min difference in retention time for Fe_3Cit_3 between xylem sap samples (**Fig. 4**) and standards (**Fig. 1**) in both HPLC systems was likely due to matrix effects. It should be noted that although the Fe_3Cit_3 complex was detected in standard solution as a mixture of two ions $[Fe_3Cit_3H]^{2-}$ and $[Fe_3OCit_3H_3]^{2-}$, in xylem sap only the latter was found. No other Fe-containing molecular ions, including Fe–NA, were found in the whole HPLC–ESI-TOFMS run using these HPLC conditions. However, using an HPLC–ESI-TOFMS method designed for Fe-*o,o*EDDHA analysis (Orera et al. 2009) a very low concentration of this Fe chelate (0.3±0.1 μM; $n=4$) was found. The Fe_3Cit_3 complex was also found in xylem sap of Fe-deficient plants resupplied with Fe-EDTA for 12 h, as well as in that of plants resupplied

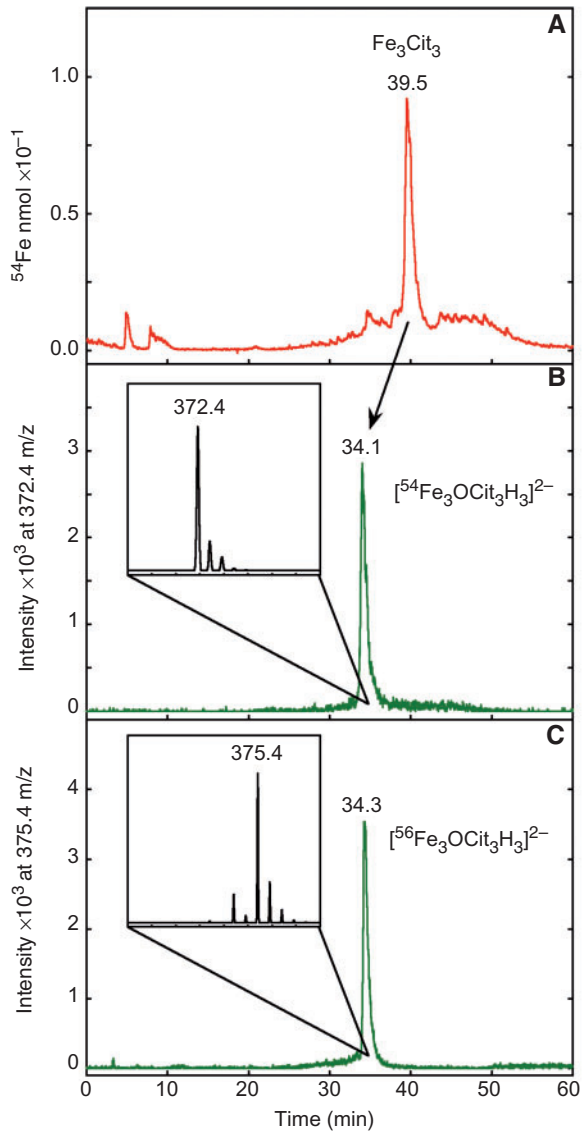

Fig. 4 HPLC–ICP-MS (A) and HPLC–ESI-TOFMS (B, C) typical chromatograms of xylem sap samples from Fe-deficient, 12-h Fe-resupplied tomato plants, showing the peak corresponding to the Fe_3Cit_3 complex. Plants were resupplied with ^{54}Fe–*o,o*EDDHA (A, B) or ^{nat}Fe–*o,o*EDDHA (C). HPLC–ESI-TOFMS traces were extracted at m/z values 372.40 and 375.40 (±0.05), corresponding to $[^{54}Fe_3OCit_3H_3]^{2-}$ and $[^{56}Fe_3OCit_3H_3]^{2-}$. Isotopic signatures of both molecular ions are shown in insets in (B) and (C).

with Fe-*o,o*EDDHA for 6 and 24 h (data not shown). However, no Fe-containing compounds could be detected in the xylem of Fe-deficient and Fe-sufficient plants.

We also attempted to quantify the amount of Fe associated with the Fe_3Cit_3 complex found in the xylem of the ^{54}Fe–*o,o*EDDHA 12 h-resupplied plants by using HPLC–ICP-MS ^{54}Fe molar flow chromatograms ($n = 3$). In these xylem samples >95% of the total Fe was ^{54}Fe. Only 25% of the injected Fe eluted from the column. The $^{54}Fe_3Cit_3$ peak accounted for the 71% of the eluted Fe and 16% of the injected Fe (**Table 2**).

Method sensitivity for the Fe_3Cit_3 complex

The sensitivity of the HPLC–ESI-TOFMS and HPLC–ICP-MS methods for the detection of the Fe_3Cit_3 complex in xylem sap can be estimated from the signal to noise ratios (s/n). Limits of detection and quantification are usually considered as the analyte concentrations giving s/n of 3 and 10, respectively. S/n found in xylem sap samples with total Fe concentrations of approximately 40 μM were 12 and 6 in HPLC–ESI-TOFMS and HPLC–ICP-MS, respectively. Therefore, in xylem sap with Fe:Cit ratios favouring the formation of Fe_3Cit_3 (>1:10; **Fig. 3**), an Fe concentration of approximately 25–30 μM will be needed for the Fe_3Cit_3 complex to be detected.

Molecular modeling of the Fe_3Cit_3 complex: an oxo-bridged tri-Fe(III) core complex

Molecular modeling of the Fe_3Cit_3 complex was carried out using the information gained from the molecular identification in xylem sap samples of Fe-deficient plants resupplied with Fe and on the basis of the known basic structure of Fe(III) carboxylates (Lippard 1988). The complex Fe_3Cit_3 has a molecular mass of 750.83 Da, a molecular formula of $Fe_3C_{18}H_{15}O_{22}$, is composed of three Cit molecules, three Fe atoms and one O atom and has two negative charges. The complex was modeled using Density Functional Theory (DFT), which has become the standard method for quantum chemical modeling of transition metals including those of biological relevance (Deeth et al. 2009 and references therein), as a trinuclear Fe(III) oxo-bridged complex (**Fig. 5, Supplementary Fig. 5**). The three Fe atoms form an equilateral triangle with an O atom in the center bridging all of them. All Fe atoms have a slightly distorted octahedral configuration. In each of the three Cit molecules, both distal carboxylate groups are bound to two Fe atoms. The four O atoms of the Cit distal carboxylate groups (two from each Cit molecule) are in the same plane of the Fe atom they complex. The two remaining positions of the Fe atom are occupied by the central carboxylate group of a Cit molecule and the O of the oxo-bridged 3-Fe center. This compact molecular geometry is further stabilized by the formation of hydrogen bonds between the hydroxyl groups and the free O atoms in the central carboxylates. Until now, six Fe–Cit complexes (three mononuclear and two dinuclear found in concentrated standard solutions, plus a nonanuclear one) have been isolated and structurally characterized in solid state (Gautier-Luneau et al. 2005 and references therein), and none of them has a central μ_3 oxygen coordinated to three Fe atoms. The Fe_2Cit_2 complex found only in Fe–Cit standard solutions was also modeled (see **Supplementary Figs. 7, 8, Supplementary Table 3**) according to the known structural characteristics found in solid state by Gautier-Luneau et al. (2005) and references therein.

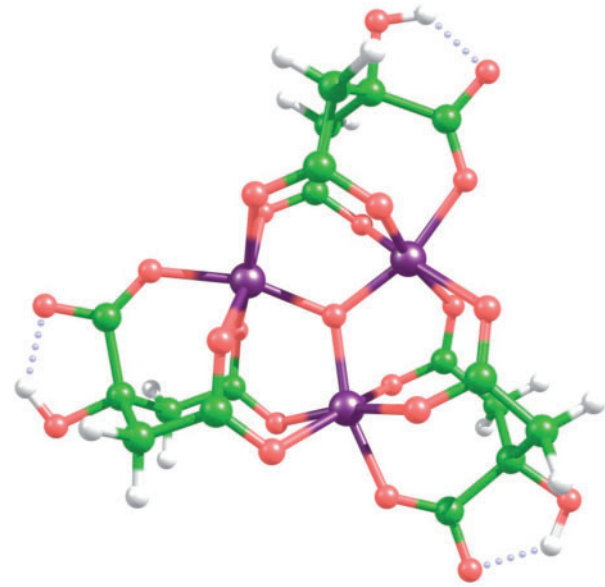

Fig. 5 Proposed structure for the Fe_3Cit_3 found in plant xylem as an oxo-bridged tri-iron–citrate complex. Iron, oxygen, carbon and hydrogen atoms are shown in purple, red, green and white, respectively.

Discussion

We report here the first direct and unequivocal identification of a natural Fe complex in plant xylem sap, Fe_3Cit_3. The complex was modeled as having an oxo-bridged tri-Fe(III) core. This is the first time that an Fe–Cit complex has been identified in biological systems. The Fe_3Cit_3 complex was identified using an integrated MS approach, based on exact molecular mass, isotopic signature, Fe content and retention time. This complex was not predicted to occur in previous in silico xylem speciation studies (López-Millán et al. 2000, López-Millán et al. 2001). A second Fe–Cit complex, Fe_2Cit_2, was also found along with Fe_3Cit_3 in standard solutions at xylem-typical pH values, with their respective abundances being tuned by the Fe:Cit ratio. The detection of Fe_3Cit_3 in the xylem sap was made possible by the use of: (i) pH values similar to those of the xylem sap throughout the analysis, (ii) a zwitterionic hydrophilic interaction column that allows for the separation of Cit and Fe–Cit complexes, (iii) high-resolution detection techniques such as ICP-MS and ESI-TOFMS, and (iv) stable Fe isotopes for identification and quantification purposes.

The changes in Fe:Cit ratios in standard solutions drive the balance between the Fe_2Cit_2 and Fe_3Cit_3 complexes, with ratios of >1:10 favoring the formation of Fe_3Cit_3 and ratios of <1:75

favoring the formation of Fe_2Cit_2 (**Fig. 3**). In the xylem sap of Fe-deficient tomato plants resupplied with Fe for 12 h, where the Fe:Cit ratio was approximately 1:1 (**Table 2**), the only complex observed was Fe_3Cit_3. The xylem sap Fe:Cit ratios in Fe-sufficient and Fe-deficient plants were approximately 1:1 and 1:30, and therefore the expected Fe–Cit complexes would be Fe_3Cit_3 and a mixture of the Fe_2Cit_2 and Fe_3Cit_3 complexes, respectively. However, no Fe–Cit complexes could be detected by HPLC–ESI-TOFMS or HPLC–ICP-MS in the xylem of these plants, likely because concentrations were below the limit of detection, estimated as approximately 25–30 µM Fe–Cit. In fact, xylem total Fe concentrations were approximately 20 and 5 µM in Fe-sufficient and Fe-deficient plants, respectively, much lower than the 43–121 µM found in Fe-deficient plants resupplied with Fe where the complex was detected. Limits of detection (LODs) for these Fe–Cit complexes are considerably higher than that reported also in xylem sap and with similar analytical techniques for the synthetic Fe chelate Fe(III)–*o,o*EDDHA, which is <1 µM (Orera et al. 2009). This supports that further analytical efforts should be made to improve the LODs for the determination of Fe–Cit complexes in plant fluids, taking into account that Fe–Cit complexes could be very sensitive to external conditions and may decompose during chromatography. Also, since the potential occurrence of other Fe compounds along with Fe–Cit complexes could explain the mass balance results found in both standard solutions and xylem sap, further analytical efforts should be made to completely speciate Fe in xylem sap.

The finding that at least an Fe–Cit complex, Fe_3Cit_3, participates in long-distance xylem Fe transport in plants is in line with what is known to occur in other organisms. In humans most of the Fe is usually chelated by transferrin, but the serum of patients with Fe overload disorders may have up to 10 µM Fe not bound to transferrin (at pH 7.4, with 100 µM Cit and an Fe:Cit ratio of 1:10) (Evans et al. 2008). This Fe fraction was proposed to consist of a mixture of oligomeric, dimeric and possibly monomeric Fe species, using a different approach from that used here. The Fe:Cit ratio in serum has also been proposed to control the balance between Fe–Cit species, with Fe:Cit ratios of >1:10 leading to oligomeric and polymeric Fe species and <1:100 leading to monomeric and dimeric Fe species (Evans et al. 2008). This framework is similar to the one we propose here for plant xylem sap, with high Fe:Cit ratios leading to Fe_3Cit_3 and low ratios leading to Fe_2Cit_2. In the bacterial plasma membrane a Fe_2Cit_2 complex is thought to be transported by the coordinated action of FecABCDE proteins (Mahren et al. 2005) where Fe_2Cit_2 binds to FecA in the outer membrane and initiates two independent processes, Fe–Cit transport into the periplasm and transcriptional induction of the *fecABCDE* genes (Yue et al. 2003). Fe–Cit transport by proteins of the CitMHS family has also been recently described in bacteria (Lensbouer et al. 2008).

The idea that Fe could be transported in the plant xylem by organic acids was first suggested many years ago (Rogers 1932), based on the ability of Fe to form stable complexes with organic acids and on the increase in these carboxylates with Fe deficiency (see Abadía et al. 2002 for a review). Pioneering studies by Brown and co-workers proposed that Fe and Cit were associated in some way, in different plant species, from the co-migration of Fe and Cit during electrophoresis and the increase in xylem Cit concentration with Fe deficiency (Brown and Tiffin 1965, Tiffin 1966a, Tiffin 1966b, Tiffin 1970, Clark et al. 1973). The first in silico xylem Fe speciation studies also suggested a major role for Cit in the complexation of Fe in tomato and soybean (White et al. 1981a, White et al. 1981b, Mullins et al. 1986). More recently, in silico studies incorporating the stability constants of other possible Fe chelators (e.g. NA), also support that Cit, rather than NA, could play a major role in Fe xylem transport (von Wirén et al. 1999, López-Millán et al. 2000, López-Millán et al. 2001, Rellán-Álvarez et al. 2008), and this was also supported by ESI-TOFMS direct determination of Fe–NA complexes in standard solutions containing Fe, NA and Cit at typical xylem pH values (Rellán-Álvarez et al. 2008). We have reviewed previous studies reporting xylem Fe and Cit concentrations to explore the likelihood of finding the Fe–Cit complexes in xylem sap (**Supplementary Table 1**). Within a given plant species, Fe:Cit ratios were generally higher in Fe-sufficient than in Fe-deficient plants, and when plants were resupplied with Fe even higher Fe:Cit ratios were found (**Supplementary Table 1**). A comparison of these Fe:Cit ratios with the threshold values proposed in this study with standard solutions (1:10 for >75% Fe_3Cit_3 and 1:75 for >75% Fe_2Cit_2) suggest that the Fe_3Cit_3 complex may occur in a wide range of species regardless of Fe nutrition status. On the other hand, the Fe_2Cit_2 complex may be prevalent in xylem sap samples with Cit concentrations in the mM range, such as those of some Fe-deficient plant species (**Supplementary Table 1**).

Recent molecular evidence also supports that Cit may be involved in long-distance Fe transport. Two *Arabidopsis thaliana* and rice mutants with altered root vasculature Cit transporters show decreases in the xylem sap concentrations of Fe and Cit, increased Fe deficiency symptoms and Fe accumulation in the root (Durrett et al. 2007, Yokosho et al. 2009). Changes found in Fe and Cit concentrations do not support that changes in Fe–Cit speciation may occur, since Fe_3Cit_3 would be expected to occur both in the wild type and mutant genotypes of both species (**Supplementary Table 1**). The phenotype of these mutants could result from a hampered Fe xylem transport, and/or from the decrease in xylem C transport itself, that may in turn impair the ability of the mutant plants to elicit root responses to Fe deficiency. Carbon fixation in roots by phosphoenolpyruvate carboxylase and export in the xylem have been proposed to play a role in the plant responses when leaf C fixation is decreased by Fe deficiency (López-Millán et al. 2000, Zocchi et al. 2007).

The central oxo-bridged tri-Fe(III) core bridged by citrate ligands of the Fe_3Cit_3 complex proposed here to occur in the xylem sap is structurally related to the active sites of numerous polyiron–oxo proteins (Tshuva and Lippard 2004). Di-Fe sites are found in a functionally diverse class of proteins which are

activated by oxygen binding and catalyze hydroxylation, desaturation and epoxidation reactions on a variety of alkyl and aryl substrates. A di-Fe site in ribonucleotide reductase, which participates in DNA biosynthesis, is responsible for the formation of organic radicals, whereas ferritins are important for Fe oxidation, storage and transport (see Tshuva and Lippard 2004 and references therein). This is the first time that a small molecule containing an oxo-bridged tri-Fe center has been reported in a biological system. We may speculate that the oxo-bridge structure may confer redox properties to this plant Fe transport form. In fact, the lowest unoccupied molecular orbital of the complex, obtained by DFT calculations, displays an energy of 1.5 eV, which is rather low for a dianionic species and indicates that the reduction of this trinuclear species could be feasible.

The finding of this negatively double charged, relatively large (750.83 Da) Fe_3Cit_3 complex opens new possibilities to re-examine the long-distance transport of Fe in the plant xylem. Very little is still known about the mechanisms of Fe xylem unloading, although it is accepted that a direct flow of Fe could occur through plasmodesmata into xylem parenchyma cells, and a second mechanism could proceed to the leaf mesophyll apoplast (Kim and Guerinot 2007, Palmer and Guerinot 2009). The molecular size of Fe_3Cit_3, 1.1×0.4 nm, would permit direct passage through plasmodesmata, which usually allows trafficking of molecules <2 nm. Once in the xylem parenchyma cytoplasm, the prevailing pH change would favor ligand exchange reactions with NA, leading to the formation of Fe–NA complexes (von Wirén et al. 1999, Rellán-Álvarez et al. 2008). Xylem Fe unloading can also proceed directly to the apoplast, where the Fe_3Cit_3 complex is also likely to occur [considering apoplast chemical composition (Kim and Guerinot 2007, Palmer and Guerinot 2009)] and will probably function as a suitable substrate for the mesophyll cell leaf plasma membrane Fe(III) chelate reductase. As mentioned above this complex is likely to have redox activity, and the oxo-bridge may play a role in the interaction with the reductase enzyme. In fact, low Fe:Cit ratios—favoring the presence of Fe_3Cit_3—seem to be optimal for leaf plasma membrane Fe(III)-chelate reductase activity, since 20-fold increases were observed when Fe:Cit ratios increased from 1:500 to 1:5 (González-Vallejo et al. 1999). Also, the complex may be a natural substrate of the root Fe(III)-chelate reductase, since it is known that root Cit excretion occurs in many plant species under Fe deficiency (Abadía et al. 2002).

Materials and Methods

Plant culture

Tomato (*Solanum lycopersicum* Mill. cv. 'Tres Cantos') plants were grown in a growth chamber with a photosynthetic photon flux density of 350 µmol m^{-2} s^{-1} photosynthetically active radiation, and a 16/8 h photoperiod, 23/18°C day/night temperature regime. Seeds were germinated and grown in vermiculite for 2 weeks. Seedlings were grown for an additional 2-week period in half-strength Hoagland nutrient solution with 45 µM ^{nat}Fe(III)–ethylenediamine tetraacetic acid (EDTA), and then transplanted to 10-liter plastic buckets (18 plants per bucket) containing half-strength Hoagland nutrient solution, pH 5.5, with either 0 (Fe-deficient plants) or 45 µM Fe(III)–EDTA (Fe-sufficient plants). Throughout this study we use ^{nat}Fe to refer to Fe with the natural isotopic composition: 5.85, 91.75, 2.12 and 0.28% of ^{54}Fe, ^{56}Fe, ^{57}Fe and ^{58}Fe, respectively. After 10 d, Fe-deficient plants were resupplied with Fe by transfer to nutrient solution with Fe [45 µM either ^{nat}Fe(III)–*o*,*o*EDDHA, ^{54}Fe(III)–*o*,*o*EDDHA or ^{nat}Fe(III)–EDTA]. Iron-54 was purchased as Fe_2O_3 (98% Fe, 95% ^{54}Fe; Cambridge Isotope Labs, Andover, MA, USA). Xylem was sampled from Fe-deficient, Fe-sufficient and Fe-deficient plants resupplied with Fe for 6, 12 and 24 h.

Xylem sap sampling

Tomato xylem sap was sampled using the detopping technique (López-Millán et al. 2009). Plant shoots were cut just below the first true leaf using a razor blade, and xylem sap was left to exude. The sap of the first 5 min was discarded to avoid contamination, the surface was washed with distilled water and blotted dry, and sap was then directly collected for 20 min using a micro-pipet and maintained in Eppendorf tubes kept on ice. Immediately after sample collection, the pH of the samples was measured with a Biotrode pH microelectrode with Idrolyte electrolyte (Metrohm, Herisau, Switzerland), tested for cytosolic contamination as indicated below and kept frozen at −80°C until further analysis. All samples were assessed for cytosolic contamination using c-mdh (EC 1.1.1.37) as a cytosolic contamination marker (López-Millán et al. 2000), and no contamination was found. Before analysis, samples were thawed and diluted 2-fold with 10 mM ammonium acetate in methanol at pH 6.8. The actual pH value of this organic mixture is estimated to be 5.5 (Canals et al. 2001). Then, samples were vortexed, centrifuged at 12 000 × *g* for 2 min and the supernatant immediately analyzed.

Fe–Cit standard solutions preparation

Iron-Cit standard solutions at different Fe:Cit ratios were prepared by adding the appropriate amounts of Fe (^{nat}Fe or ^{54}Fe) to Cit solutions prepared in 10 mM ammonium acetate at pH 5.5. Fe–Cit solutions were gently vortexed, diluted 2-fold with 10 mM ammonium acetate in methanol at pH 6.8 and immediately analyzed. The pH value of this organic mixture is estimated to be 5.5 (Canals et al. 2001).

Analysis of Fe complexes by HPLC coupled to electrospray ionization MS

Chromatographic separation was performed on a modified Alliance 2795 HPLC system (Waters, Mildford, MA, USA). The fluidics system, with the exception of the pump head, was built with PEEK, and a Ti needle was used to minimize metal contamination. Different HPLC conditions were tested, including

several column types, elution programs and organic solvents (acetonitrile and methanol). Final HPLC analysis conditions were as follows. The autosampler was kept at 4°C and the column compartment temperature was set at 30°C. Injection volume was 20 µl, and a ZIC-pHILIC, 150×2.1 mm, 5 µm column (Sequant, Umea, Sweden) was used with a flow rate of 100 µl min^{-1}. The mobile phase was built using two eluents: A (10 mM ammonium acetate in water at pH 5.5) and B (10 mM ammonium acetate in methanol at pH 6.8). All mobile phase chemicals were LC-MS grade (Riedel-de Haën, Seelze, Germany). For separation, an initial equilibration time of 80% B and 20% A (from min 0 to 5) was followed by a linear gradient from 80 to 20% B (from min 5 to 20). This mobile phase composition was held for 15 min, then changed linearly to the initial conditions for 10 min, and kept as such for another 15 min. Total run time per sample was 1 h. The pH values during the HPLC run ranged from 5.3 to 6.2 depending on organic mixture composition of the mobile phase (Canals et al. 2001). Injections of 5 mM Cit (20 µl) were carried out between samples to minimize Fe cross-contamination.

High-resolution MS analysis was carried out with a micrOTOF II ESI-TOFMS apparatus (Bruker Daltoniks GmbH, Bremen, Germany) in the 50–1000 m/z range. The micrOTOF II was operated in negative mode at 3000 and −500 V capillary and end-plate voltages, respectively. After optimization, capillary exit, skimmer 1 and hexapole RF voltages were set at −57.1, −39.1 and 145.2 V, respectively. Nebulizer gas (N_2) pressure was kept at 2.0 bar and drying gas (N_2) flow was set at 8.0 liter min^{-1} with a temperature of 180°C. Mass calibration was carried out with 10 mM Li-formate solution using a syringe pump (Cole-Parmer Instruments, Vernon Hills, IL, USA). In each HPLC run mass calibration was carried out by on-line injection of 20 µl of Li-formate at 2 min. Molecular formulae were assigned based on (i) exact molecular mass, with errors <10 ppm, and (ii) the SigmaFit™ algorithm, with a threshold tolerance value of 0.03 SigmaFit™ values (Ojanperä et al. 2006). Appropriate isotopic abundances were used for the calculations. The system was controlled with the software packages MicrOTOF Control v.2.2 and HyStar v.3.2 (Bruker Daltonics). Data were processed with Data Analysis v.3.4 software (Bruker Daltonics).

Analysis of Fe and Fe complexes by ICP-MS

ICP-MS analysis was carried out with a Q-ICP-MS instrument (7500ce; Agilent Technologies, Tokyo, Japan). The instrument was fitted with an octapole collision cell system located between the ion lenses and a quadrupole MS analyzer for removal of polyatomic interference. In this study He was used as a collision gas. In addition, O_2 (7%) was added to the plasma by an additional mass flow controller to remove C excess, and to prevent it from condensing on the interface and ion lenses due to the high organic content of the mobile phase during HPLC separation (Woods and Fryer 2007). Platinum interface cones were used to allow the addition of O_2. The Q-ICP-MS instrument was operated with a RF power of 1500 W and cooling, sample and make-up gas flows of 15, 0.9 and 0.2 liter min^{-1}, respectively. The collision cell was operated with a He gas flow of 4.2 ml min^{-1} and octapole bias and QP bias voltages of −18.0 and −16.0 V, respectively. The torch position and ion lens voltage settings were optimized daily for maximum sensitivity with a 1 ng g^{-1} Li, Co, Y, Tl and Ce mixture in 1% (w/w) HNO_3 solution. A solution of 1% (w/w) HNO_3 was also used to check the background level caused by polyatomic Ar interference. The possible contribution of isobaric interference of ^{54}Cr and ^{58}Ni in the determination of the ^{54}Fe and ^{58}Fe isotopes was corrected mathematically by measuring the ion signals at masses 52 for Cr and 60 for Ni and assuming natural abundances as reported by IUPAC (De Laeter et al. 2003). Mass bias correction was carried out by measuring the isotope ratios of the ^{nat}Fe standard and calculating the mass bias factor (K) with an exponential model (Rodríguez-Castrillón et al. 2008). The ICP-MS instrument was controlled with the software packages ICP-MS ChemStation v.B.03.04 and ICP-MS Chromatographic v.B.03.04 (Agilent Technologies).

For the ICP-MS analysis of ^{54}Fe–citrate complexes in standard solutions and xylem sap samples, a chromatographic separation was performed on an Agilent 1100 chromatographic system (Agilent Technologies) using the method described for HPLC–ESI-TOFMS analysis. Iron-54 and ^{nat}Fe quantification was carried out by post-column isotope dilution analysis (IDA) (Rodríguez-González et al. 2005) with a 20 ng g^{-1} ^{57}Fe in EDTA solution continuously introduced at 0.10 g min^{-1} through a T piece connected to the end of the column and before the plasma entrance. Iron-57 was purchased as Fe_2O_3 (98% Fe, 95% ^{57}Fe; Cambridge Isotope Labs). The ICP-MS intensity chromatograms (counts s^{-1}) were converted into Fe molar flow chromatograms (^{54}Fe nmol min^{-1}) using the isotope pattern deconvolution (IPD) equations described elsewhere (Rodríguez-Castrillón et al. 2008, González Iglesias et al. 2009). Accurate isotope abundances of the ^{57}Fe and ^{54}Fe enriched solutions were determined by direct ICP-MS injections and used for these calculations. Isotope abundances (% ^{54}Fe, ^{56}Fe, ^{57}Fe and ^{58}Fe) were 0.14, 4.74, 94.63 and 0.49 in ^{57}Fe-enriched solutions and 99.67, 0.25, 0.01 and 0.06 in ^{54}Fe-enriched solutions.

Total ^{54}Fe and ^{nat}Fe determinations in xylem sap samples were carried out by direct ICP-MS injections and IDA, spiking known amounts of the characterized ^{57}Fe-enriched solution into the samples acidulated with HNO_3. Also, the mathematical IPD procedure described elsewhere (Rodríguez-Castrillón et al. 2008, González Iglesias et al. 2009) was used.

Other determinations

Citrate was analyzed by HPLC (Waters Alliance 2795) using a Supelcogel H 250×4.6 mm column. Analyses were performed isocratically at a flow rate of 200 µl min^{-1} and at a temperature of 30°C. The mobile phase was 0.1 % formic acid. Detection was performed by ESI-TOFMS (micrOTOF II; Bruker Daltonics) at 191.0 m/z. Quantification was carried out by external calibration with internal standarization (with [^{13}C]4-L-malic acid; Cambridge Isotope Laboratories). The Fe(III) chelate of *o,o*EDDHA was determined as described elsewhere (Orera et al. 2009).

Iron–citrate complex molecular modeling

All theoretical calculations were performed by using the Gaussian 03 program (Frisch et al. 2003). The molecular geometry of $(Fe_3OCit_3)^{2-}$ was optimized assuming C_{3h} symmetry. The chemistry model used consisted in the Becke's three-parameter exchange functional combined with the LYP correlation functional (B3LYP) (Becke 1993) and the LanL2DZ basis set as indicated in the Gaussian 03 program (Frisch et al. 2003). In order to achieve the convergence of the wavefunction, an initial guess was obtained using the same chemistry model on the closed shell $(Fe_3OCit_3)^{2-}$ species.

Supplementary data

Supplementary data are available at PCP online.

Funding

This work was supported by the Spanish Ministry of Science and Innovation (grant numbers AGL2006-1416, AGL2007-61948 and CTQ2006-05722, co-financed with FEDER); the European Commission (Thematic Priority 5—Food Quality and Safety, 6th Framework RTD Programme, grant number FP6-FOOD-CT-2006-016279) and the Aragón Government (groups A03 and E39). Acquisition of the HPLC–TOFMS apparatus was cofinanced with FEDER. R.R.-A., J.G.-M.-S., I.O. and J.A.R.-C. were supported by FPI-MICINN, FICYT-MICINN, CONAID-DGA and FPU-MICINN grants, respectively.

Acknowledgments

We thank Ade Calviño and Aurora Poc (Aula Dei Experimental Station–CSIC, Zaragoza, Spain) for growing the plants, Professor Jian Feng Ma (Research Institute for Bioresources, Okayama University, Kurashiki, Japan) for the kind supply of DMA and Dr. Ana-Flor López-Millán (Aula Dei Experimental Station–CSIC, Zaragoza, Spain) for critically reviewing the manuscript and helpful suggestions.

References

Abadía, J., López-Millán, A.F., Rombolà, A. and Abadía, A. (2002) Organic acids and Fe deficiency: a review. *Plant Soil* 241: 75–86.

Becke, A.D. (1993) A new mixing of Hartree-Fock and local density-functional theories. *J. Chem. Phys.* 98: 1372–1377.

Briat, J.F., Curie, C. and Gaymard, F. (2007) Iron utilization and metabolism in plants. *Curr. Opin. Plant Biol.* 10: 276–282.

Brown, J. (1966) Fe and Ca uptake as related to root-sap and stem-exudate citrate in soybeans. *Physiol. Plant.* 19: 968–976.

Brown, J.C. and Tiffin, L.O. (1965) Iron stress as related to the iron and citrate ocurring in stem exudate. *Plant Physiol.* 40: 395–400.

Canals, I., Oumada, F.Z., Rosés, M. and Bosch, E. (2001) Retention of ionizable compounds on HPLC. 6. pH measurements with the glass electrode in methanol-water mixtures. *J. Chromatogr. A* 911: 191–202.

Clark, R.B., Tiffin, L.O. and Brown, J.C. (1973) Organic-acids and iron translocation in maize genotypes. *Plant Physiol.* 52: 147–150.

Curie, C., Cassin, G., Couch, D., Divol, F., Higuchi, K., Le Jean, M., et al. (2008) Metal movement within the plant: contribution of nicotianamine and yellow stripe 1-like transporters. *Ann. Bot.* 103: 1–11.

De Laeter, J., Böhlke, J., De Bievre, P., Hidaka, H., Peiser, H., Rosman, K., et al. (2003) Atomic weights of the elements: review 2000. *Pure Appl. Chem.* 75: 683–800.

Deeth, R., Anastasi, A., Diedrich, C. and Randell, K. (2009) Molecular modelling for transition metal complexes: Dealing with d-electron effects. *Coord. Chem. Rev.* 253: 795–816.

Durrett, T.P., Gassmann, W. and Rogers, E.E. (2007) The FRD3-mediated efflux of citrate into the root vasculature is necessary for efficient iron translocation. *Plant Physiol.* 144: 197–205.

Evans, R.W., Rafique, R., Zarea, A., Rapisarda, C., Cammack, R., Evans, P.J., et al. (2008) Nature of non-transferrin-bound iron: Studies on iron citrate complexes and thalassemic sera. *J. Biol. Inorg. Chem.* 13: 57–74.

Frisch, M.J., Trucks, G.W., Schlegel, H.B., Scuseria, G.E., Robb, M.A., et al. (2003) Gaussian 03, Revision B.05. Gaussian, Inc., Pittsburgh, PA, USA.

Gautier-Luneau, I., Merle, C., Phanon, D., Lebrun, C., Biaso, F., Serratrice, G., et al. (2005) New trends in the chemistry of iron(III) citrate complexes: Correlations between X- ray structures and solution species probed by electrospray mass spectrometry and kinetics of iron uptake from citrate by iron chelators. *Chem. Europ. J.* 11: 2207–2219.

González Iglesias, H., Fernández Sánchez, M.L., Rodríguez-Castrillón, J.A., García-Alonso, J.I., Sastre, J.L. and Sanz-Medel, A. (2009) Enriched stable isotopes and isotope pattern deconvolution for quantitative speciation of endogenous and exogenous selenium in rat urine by HPLC-ICP-MS. *J. Anal. Atom. Spectrom.* 24: 460–468.

González-Vallejo, E., González-Reyes, J., Abadía, A., López-Millán, A., Yunta, F., Lucena, J., et al. (1999) Reduction of ferric chelates by leaf plasma membrane preparations from Fe-deficient and Fe-sufficient sugar beet. *Aust. J. Plant Physiol.* 26: 601–611.

Hider, R.C., Yoshimura, E., Khodr, H. and von Wiren, N. (2004) Competition or complementation: the iron-chelating abilities of nicotianamine and phytosiderophores. *New Phytol.* 164: 204–208.

Kim, S.A. and Guerinot, M.L. (2007) Mining iron: iron uptake and transport in plants. *FEBS Lett.* 581: 2273–2280.

Küpper, H., Mijovilovich, A., Meyer-Klaucke, W. and Kroneck, P.M. (2004) Tissue- and age-dependent differences in the complexation of cadmium and zinc in the cadmium/zinc hyperaccumulator *Thlaspi caerulescens* (Ganges ecotype) revealed by x-ray absorption spectroscopy. *Plant Physiol.* 134: 748–757.

Larbi, A., Morales, F., Abadía, J. and Abadía, A. (2003) Effects of branch solid Fe sulphate implants on xylem sap composition in field-grown peach and pear: changes in Fe, organic anions and pH. *J. Plant Physiol.* 160: 1473–1481.

Lensbouer, J., Patel, A., Sirianni, J. and Doyle, R. (2008) Functional characterization and metal ion specificity of the metal-citrate complex transporter from *Streptomyces coelicolor*. *J. Bacteriol.* 190: 5616–5623.

Lippard, S.J. (1988) Oxo-bridged polyiron centers in biology and chemistry. *Angew. Chem. Int. Ed.* 27: 344–361.

López-Millán, A., Morales, F., Gogorcena, Y., Abadía, A. and Abadía, J. (2009) Metabolic responses in iron deficient tomato plants. *J. Plant Physiol.* 166: 375–384.

López-Millán, A.F., Morales, F., Abadía, A. and Abadía, J. (2000) Effects of iron deficiency on the composition of the leaf apoplastic fluid and

xylem sap in sugar beet. Implications for iron and carbon transport. *Plant Physiol.* 124: 873–884.

López-Millán, A.F., Morales, F., Abadía, A. and Abadía, J. (2001) Iron deficiency-associated changes in the composition of the leaf apoplastic fluid from field-grown pear (*Pyrus communis* L.) trees. *J. Exp. Bot.* 52: 1489–1498.

Mahren, S., Schnell, H. and Braun, V. (2005) Occurrence and regulation of the ferric citrate transport system in *Escherichia coli*, *Klebsiella pneumoniae*, *Enterobacter aerogenes*, and *Photorhabdus luminescens*. *Arch. Microbiol.* 184: 175–186.

Meija, J., Montes-Bayón, M., Caruso, J. and Sanz-Medel, A. (2006) Integrated mass spectrometry in (semi-) metal speciation and its potential in phytochemistry. *Trends Anal. Chem.* 25: 44–51.

Mullins, G.L., Sommers, L.E. and Housley, T.L. (1986) Metal speciation in xylem and phloem exudates. *Plant Soil.* 16: 377–391.

Nikolic, M. and Römheld, V. (1999) Mechanism of Fe uptake by the leaf symplast: Is Fe inactivation in leaf a cause of Fe deficiency chlorosis? *Plant Soil* 215: 229–237.

Ojanperä, S., Pelander, A., Pelzing, M., Krebs, I., Vuori, E. and Ojanperä, I. (2006) Isotopic pattern and accurate mass determination in urine drug screening by liquid chromatography/time-of-flight mass spectrometry. *Rapid Commun. Mass Spectrom.* 20: 1161–1167.

Orera, I., Abadía, A., Abadía, J. and Álvarez-Fernández, A. (2009) Determination of *o,o*EDDHA—a xenobiotic chelating agent used in Fe fertilizers—in plant tissues by liquid chromatography/electrospray mass spectrometry: Overcoming matrix effects. *Rapid Commun. Mass Spectrom.* 23: 1694–1702.

Ouerdane, L., Mari, S., Czernic, P., Lebrun, M. and Lobinski, R. (2006) Speciation of non-covalent nickel species in plant tissue extracts by electrospray Q-TOFMS/MS after their isolation by 2D size exclusion-hydrophilic interaction LC (SEC-HILIC) monitored by ICP-MS. *J. Anal. Atom. Spectrom.* 21: 676–683.

Palmer, C. and Guerinot, M.L. (2009) Facing the challenges of Cu, Fe and Zn homeostasis in plants. *Nat. Chem. Biol.* 5: 333–340.

Pierre, J.L. and Gautier-Luneau, I. (2000) Iron and citric acid: a fuzzy chemistry of ubiquitous biological relevance. *BioMetals* 13: 91–96.

Punshon, T., Guerinot, M.L. and Lanzirotti, A. (2009) Using synchrotron X-ray fluorescence microprobes in the study of metal homeostasis in plants. *Ann. Bot.* 103: 665–672.

Rellán-Álvarez, R., Abadía, J. and Álvarez-Fernández, A. (2008) Formation of metal-nicotianamine complexes as affected by pH, ligand exchange with citrate and metal exchange. A study by electrospray ionization time-of-flight mass spectrometry. *Rapid Commun. Mass Spectrom.* 22: 1553–1562.

Rodríguez-Castrillón, J.A., Moldován, M. and Encinar, J.R. (2008) Isotope pattern deconvolution for internal mass bias correction in the characterisation of isotopically enriched spikes. *J. Anal. Atom. Spectrom.* 23: 318–324.

Rodríguez-González, P., Marchante-Gayón, J., García Alonso, J. and Sanz-Medel, A. (2005) Isotope dilution analysis for elemental speciation: a tutorial review. *Spectrochim. Acta B* 60: 151–207.

Rogers, C. (1932) Factors affecting the distribution of iron in plants. *Plant Physiol.* 7: 227–252.

Sarret, G., Saumitou-Laprade, P., Bert, V., Proux, O., Hazemann, J.L., Traverse, A., et al. (2002) Forms of zinc accumulated in the hyperaccumulator *Arabidopsis halleri*. *Plant Physiol.* 130: 1815–1826.

Spiro, T., Bates, G. and Saltman, P. (1967a) Hydrolytic polymerization of ferric citrate. II. Influence of excess citrate. *J. Am. Chem. Soc.* 89: 5559–5562.

Spiro, T., Pape, L. and Saltman, P. (1967b) Hydrolytic polymerization of ferric citrate. I. Chemistry of the polymer. *J. Am. Chem. Soc.* 89: 5555–5559.

Tiffin, L.O. (1966a) Iron translocation. I. Plant culture exudate sampling iron-citrate analysis. *Plant Physiol.* 41: 510–514.

Tiffin, L.O. (1966b) Iron translocation. II. Citrate/iron ratios in plant stem exudates. *Plant Physiol.* 41: 515–518.

Tiffin, L.O. (1970) Translocation of iron citrate and phosphorus in xylem exudate of soybean. *Plant Physiol.* 45: 280–283.

Tiffin, L.O. and Brown, J.C. (1962) Iron chelates in soybean exudate. *Science* 135: 311–313.

Tshuva, E. and Lippard, S. (2004) Synthetic models for non-heme carboxylate-bridged diiron metalloproteins: Strategies and tactics. *Chem. Rev.* 104: 987–1012.

von Wirén, N., Klair, S., Bansal, S., Briat, J.F., Khodr, H., Shioiri, T., et al. (1999) Nicotianamine chelates both FeIII and FeII. Implications for metal transport in plants. *Plant Physiol.* 119: 1107–1114.

White, M.C., Baker, F.D., Chaney, R.L. and Decker, A.M. (1981a) Metal complexation in xylem fluid: II. Theoretical equilibrium and computational computer program. *Plant Physiol.* 67: 301–310.

White, M.C., Decker, A.M. and Chaney, R.L. (1981b) Metal complexation in xylem fluid: I. Chemical composition of tomato and soybean exudate. *Plant Physiol.* 67: 292–300.

Woods, G.D. and Fryer, F.I. (2007) Direct elemental analysis of biodiesel by inductively coupled plasma-mass spectrometry. *Anal. Bioanal. Chem.* 389: 753–761.

Xuan, Y., Scheuermann, E.B., Meda, A.R., Hayen, H., von Wirén, N. and Weber, G. (2006) Separation and identification of phytosiderophores and their metal complexes in plants by zwitterionic hydrophilic interaction liquid chromatography coupled to electrospray ionization mass spectrometry. *J. Chromatogr. A* 1136: 73–81.

Yokosho, K., Yamaji, N., Ueno, D., Mitani, N. and Ma, J.F. (2009) OsFRDL1 is a citrate transporter required for efficient translocation of iron in rice. *Plant Physiol.* 149: 297–305.

Yue, W.W., Grizot, S. and Buchanan, S. (2003) Structural evidence for iron-free citrate and ferric citrate binding to the TonB-dependent outer membrane transporter FecA. *J. Mol. Biol.* 332: 353–368.

Zocchi, G., De Nisi, P., Dell'Orto, M., Espen, L. and Gallina, P.M. (2007) Iron deficiency differently affects metabolic responses in soybean roots. *J. Exp. Bot.* 58: 993–1000.